

Resonant Electro-Optic Frequency Comb

Alfredo Rueda

Max Planck Institute for the Science of Light, Staudtstr. 2, 90158 Erlangen, Germany

Institute for Optics, Information and Photonics,

University Erlangen-Nuernberg, Staudtstr. 7/B2, 91058 Erlangen, Germany

SAOT, School in Advanced Optical Technologies, Paul-Gordan-Str. 6, 91052 Erlangen, Germany

Institute of Science and Technology Austria, am Campus 1, 3600 Klosterneuburg, Austria and

The Dodd-Walls Centre for Photonic and Quantum Technologies,

Department of Physics, University of Otago, Dunedin, New Zealand

Florian Sedlmeir and Gerd Leuchs

Max Planck Institute for the Science of Light, Staudtstr. 2, 90158 Erlangen, Germany and

Institute for Optics, Information and Photonics,

University Erlangen-Nuernberg, Staudtstr. 7/B2, 91058 Erlangen, Germany

Madhuri Kumari and Harald G. L. Schwefel*

The Dodd-Walls Centre for Photonic and Quantum Technologies,

Department of Physics, University of Otago, Dunedin, New Zealand

(Dated: August 7, 2018)

High speed optical telecommunication is enabled by wavelength division multiplexing, whereby hundreds of individually stabilized lasers encode the information within a single mode optical fiber. In the seek for larger bandwidth the optical power sent into the fiber is limited by optical non-linearities within the fiber and energy consumption of the light sources starts to become a significant cost factor [1]. Optical frequency combs have been suggested to remedy this problem by generating multiple laser lines within a monolithic device, their current stability and coherence lets them operate only in small parameter ranges [2–4]. Here we show that a broadband frequency comb realized through the electro-optic effect within a high quality whispering gallery mode resonator can operate at low microwave and optical powers. Contrary to the usual third order Kerr non-linear optical frequency combs we rely on the second order non-linear effect which is much more efficient. Our result uses a fixed microwave signal which is mixed with an optical pump signal to generate a coherent frequency comb with a precisely determined carrier separation. The resonant enhancement enables us to operate with microwave powers three order magnitude smaller than in commercially available devices. We can expect the implementation into the next generation long distance telecommunication which relies on coherent emission and detection schemes to allow for operation with higher optical powers and at reduced cost [5].

The internet data capacity is projected to increase by a factor of two every year [6], and the current optical

carriers are not able to meet the rising demand of expansion in the bandwidth of the undersea fibre network [7]. Techniques like space division multiplexing [8], mode-division multiplexing [9] and wavelength division multiplexing (WDM) [5] are being researched to exploit the existing network to its full capacity. The current WDM systems employ an array of individually stabilized lasers, that are not phase locked to each other. For the next generation a major shift in the paradigm from multiple independent optical carriers to coherent optical frequency combs (OFCs) [7] is on its way where the coherent OFCs can be generated from a single optical carrier. Some of the important features of OFCs like phase and frequency stability, tunability of comb spacing, and power conversion efficiency depend upon the method of generation. Especially the phase locking of all comb lines is particularly interesting for future WDM applications as novel coherent detection methods allow to counter one of the main limitations for higher optical powers within the telecommunication fibres [5]. Standard OFCs are based on fs-laser [10, 11], but recently small micro-resonator based frequency combs based on the Kerr non-linearities (a third order nonlinearity) [11–14] have shown huge successes.

A different approach is electro-optic modulation (EOM) [21] based on second order non-linearities [22]. This scheme exploits second-order non-linearity, whereby two continuous waves, e.g. one in the optical range (carrier) and one in the microwave range (modulating wave) are sent into a non-linear non-centrosymmetric material. In the past, over-driving of conventional electro-optic modulators was explored for comb generation [23–26]. These EOM based combs have unique advantages having tunable central-frequency and comb-line spacing which are crucial for a range of applications. However, these combs suffer from inherent phase instabilities and excess multiplication of microwave phase noise which restricts

* harald.schwefel@otago.ac.nz

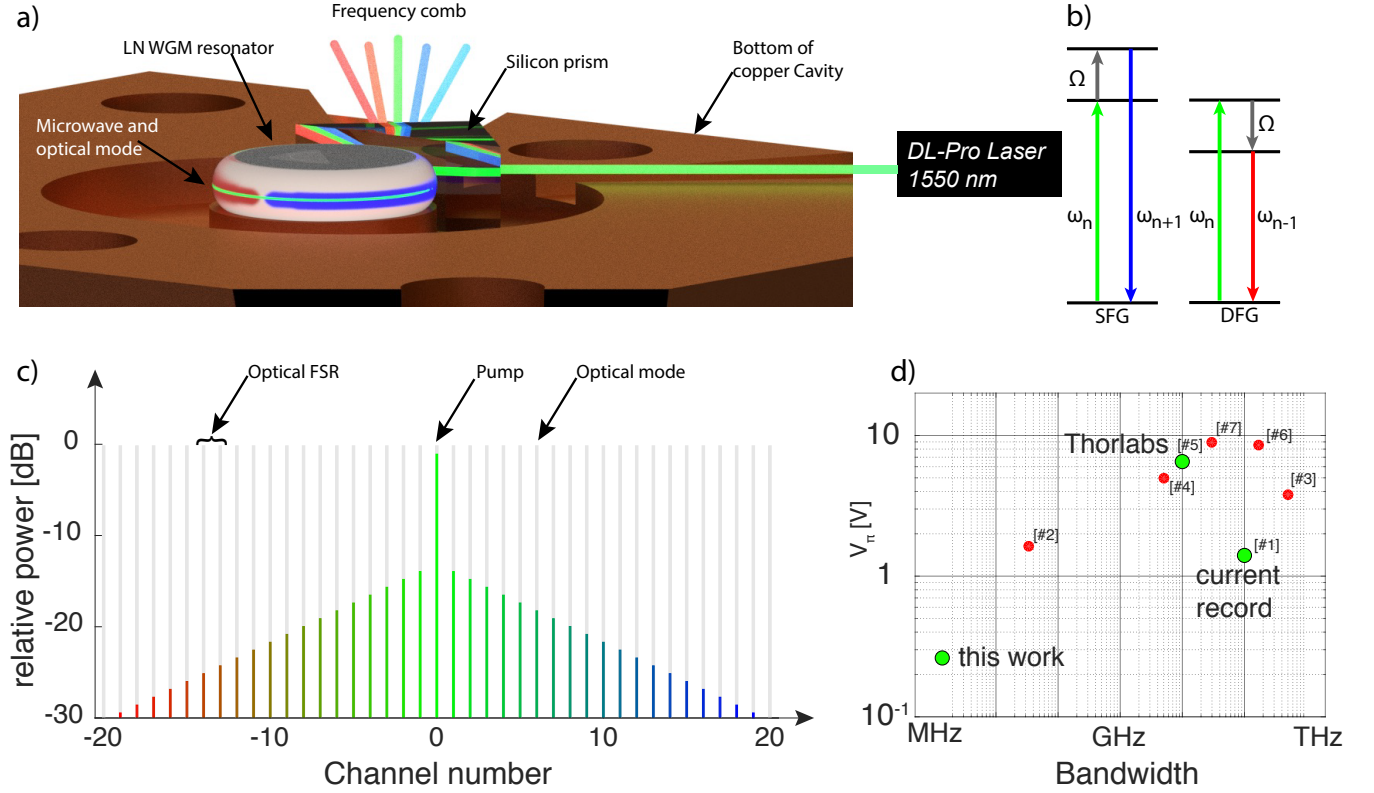


FIG. 1. **Principles of $\chi^{(2)}$ WGM-based frequency combs generation** a) Artistic illustration of creation of $\chi^{(2)}$ -frequency combs using a multi-resonant system. The pump coming from a commercial telecom laser is coupled to a LiNbO₃-WGM resonator, which provides a multimode optical system with nearly constant optical free spectral range (FSR). The microwave tone is coupled into the 3D copper cavity with the WGM resonator clamped at its center. This hybrid system is resonant at the frequency of the optical FSR (8.9 GHz) and the mode profile is strongly confined at the rim of the resonator, increasing the mode overlap. The wave mixing process happens in the resonator creating the comb. The new created sidebands are outcoupled through the prism for later processing. b) Energy scheme for the sum (and difference) frequency generation in which any given mode of angular momentum m only interacts with its neighbours $m + 1$ and $m - 1$. c) Illustration of the theoretical spectrum of the normalized $\chi^{(2)}$ frequency comb as function of the sideband order. The optical modes are separated by a constant FSR which matches the microwave pump frequency Ω . d) Comparison of the V_π voltages for different electro-optic modulators, noting in particular that our result of $V_\pi = 260$ mV is almost an order of magnitude better than the current record of #1 Ref. [15], and 25 times better than a commercial Thorlabs modulator LN53S-FC (#5). Other notable values #2 Ref. [16], #3 Ref. [17], #4 Ref. [18], #6 Ref. [19], #7 Ref. [20].

their usage in long-distance data transfer [5].

Here, we report the first experimental demonstration of efficient resonant enhanced electro-optic comb generation. Such a fully coherent comb with intrinsic phase noise suppression allows to increase the information content and data rate. The phase stability between the comb lines is inherently given due to the fixed interaction of two stable sources. Our experiment draws on an in-depth theoretical description of the resonantly enhanced non-linear interaction and we show in a first experiment the potential of this method by reporting on a coherent comb with 8.9 GHz spacing spanning a section of more than one hundred lines in the C-Band (1530 nm – 1565 nm) with only 20 dBm of microwave modulation power. The results clearly demonstrate a resurgence of

EOM and shows the large potential of resonantly enhance electro-optic modulation for the next generation of ultra dense WDM.

Our scheme is illustrated in Fig. 1 a) where a whispering gallery mode (WGM) resonator enhances the non-linear interaction between the optical pump field and microwave field. This interaction is mediated by a phase modulation, which originates from the field dependence of the refractive index commonly known as the Pockels effect and creates sidebands symmetrically around the optical pump frequency (see Fig. 1 b) and c). WGM resonators confine light due to the total internal reflection at the dielectric-air boundary and are particularly suited for resonant enhancement as they can confine both optical and high frequency microwave radiation in the same

small mode volume [27–29]. Analytically optical WGMs can be described by three parameters identified as angular number m (number of wavelengths around the rim of the resonator), polar number p , and radial number q (see Supplement). Resonators made out of a suitable low loss non-linear materials allow for long confinement times $\tau_p = 1/2\Gamma_0$, where Γ_0 is the total field loss rate and related to the resonator quality factor $Q = \omega_0\tau_p$, with ω_0 the angular frequency of the mode. The optical confinement times τ_p can be in the order of the hundreds of nanosecond [28, 30] corresponding to Q above 100 millions. Another important factor is the free spectral range (FSR) which is the inverse of the round trip time in the cavity given by [31–33] $\text{FSR} = 1/\tau = 2\pi nR/c$ with R as the radius of the WGM-resonator. For mm-sized resonators the FSR's are in the order of GHz and they remain almost equidistant in a range of some hundreds of pm, limited by the dispersion of the refractive index.

Microwave WGM in non-linear materials have shown material limited Q -factors in the order of $10^4 - 10^5$ [34]. Microwaves, due to their long wavelength, are however poorly confined in mm-sized WGM resonators in free space, therefore decreasing the overlap with the optical modes, and thus the non-linear interaction. In order to confine them we use a coupled system based on a 3D-microwave cavity and a WGM resonator. This hybrid system gives us a higher degree of freedom to control the microwave spatial distribution $\psi_\Omega(\vec{r})$, microwave resonance frequency Ω_0 and coupling rate γ_Ω . We choose a monolithic lithium niobate (LiNbO_3) resonator clamped between two copper ring electrodes inside a copper cavity. Then, the microwave electric field is focused between the upper and lower ring electrodes, similar to a capacitor, with the rim of the WGM resonator in between. In this way we maximize the microwave electric field at the spot of the optical modes. The rest of the cavity inner volume, can be varied to get the desired microwave resonance frequency (see Fig.1 a) for a schematic of the bottom half of the cavity). We optimize the cavity geometry and extract information such as the resonance frequency, internal Q'_Ω factor, coupling rate, mode volume and the electric field of a single photon for different disk thickness through numerical simulations with COMSOL (see Supplement). We note that this hybrid system is almost identical to our previous work on coherent microwave up-conversion, showing the versatility of this setup [28].

The physical description of the electro-optic process is classified under the second order non-linear electric susceptibility $\chi^{(2)}$. In the energy description of light both interacting fields can be added resulting in sum frequency generation (SFG) and difference frequency generation (DFG). The process of SFG combines a microwave and an optical photon and creates a blue-shifted photon (anti-Stokes). In the process of DFG, the microwave signal photon can stimulate an optical pump photon to decay into a red-shifted optical (Stokes) and an additional microwave photon. In the supplement we derive the Hamiltonian of the system where the interaction be-

tween the modes is summarized in the non-linear coupling constant g and depends on the parameters: modal overlap, phase matching, and the effective electro-optic coefficient. We can interpret g as the photon conversion rate from the pump mode to the sideband mode per pump photon:

$$g = 2\epsilon_0\chi^{(2)}\sqrt{\frac{\hbar\Omega\omega_p\omega_s}{8\epsilon_\Omega\epsilon_p\epsilon_sV_\Omega V_p V_s}}\int dV\psi_s^\dagger\psi_p\psi_\Omega, \quad (1)$$

with ϵ_i the permittivity, V_i the effective mode volume and ψ_i the normalized mode distribution of the participating waves (with $i = (\Omega, p, s)$ corresponding to the microwave, pump, and signal field, respectively). Besides the energy conservation the angular momentum also needs to be conserved. In Eq. (1) it is the final integral that leads to Clebsch-Gordan like conservation laws [35] with only non-zero g if the angular momentum numbers of the interacting fields obey the relation $m_s = m_p \pm m_\Omega$. Figure 1 a) shows schematically how the microwave field of $m_\Omega = 1$ oscillates in the WGM. The figure of merit in electro-optic modulator is usually given by the π -voltage (V_π), which is the voltage required to shift the carrier phase by π at given frequency. In our system the carrier single round trip phase shift over the round trip time per microwave photon is given by g [36]. In a resonant system the carrier is confined in the WGM-resonator an average time τ_p and using the relation between voltage and mean photon number (see Supplement), the π -voltage can be calculated as:

$$V_\pi = \frac{\pi}{g\tau_p}\sqrt{\frac{Zh\Omega(\gamma_\Omega + \gamma'_\Omega)^2}{\gamma_\Omega}}, \quad (2)$$

where Z , γ_Ω and γ'_Ω stand for the impedance, microwave field coupling rate and microwave field intrinsic loss rate, respectively. In our proposed system with a WGM resonator of $R = 2.4$ mm and disk thickness $h = 400$ μm , with FSR of $2\pi \times 8.9$ GHz under the assumptions of critical microwave coupling and an optical loaded Q -factor in the order of 10^8 at the optical frequency $\omega_0 = 2\pi \times 193.5$ THz and microwave resonance frequency Ω around $2\pi \times 8.9$ GHz we obtain V_π in the range of few tens of mV (see Supplement). In Fig. 1 d) we compare V_π values to their bandwidth for different realizations. Our values are a tremendous improvement over commercial phase modulator, which have a V_π above 6.5 V at 10 GHz resulting in 422 mW of microwave power compared to our system requiring only 400 μW . The tradeoff for our system is its bandwidth which is several tens of MHz while standard commercial modulators have usually some GHz bandwidth. This however is not a limitation for our proposed frequency comb scheme that we can realise by over-driving our highly efficiency modulator at a fixed modulation frequency. We note that there is no experimental constraint to work at higher frequencies such as 12.5 GHz or 50 GHz suitable for next generation ultra dense and dense WDM, respectively, by

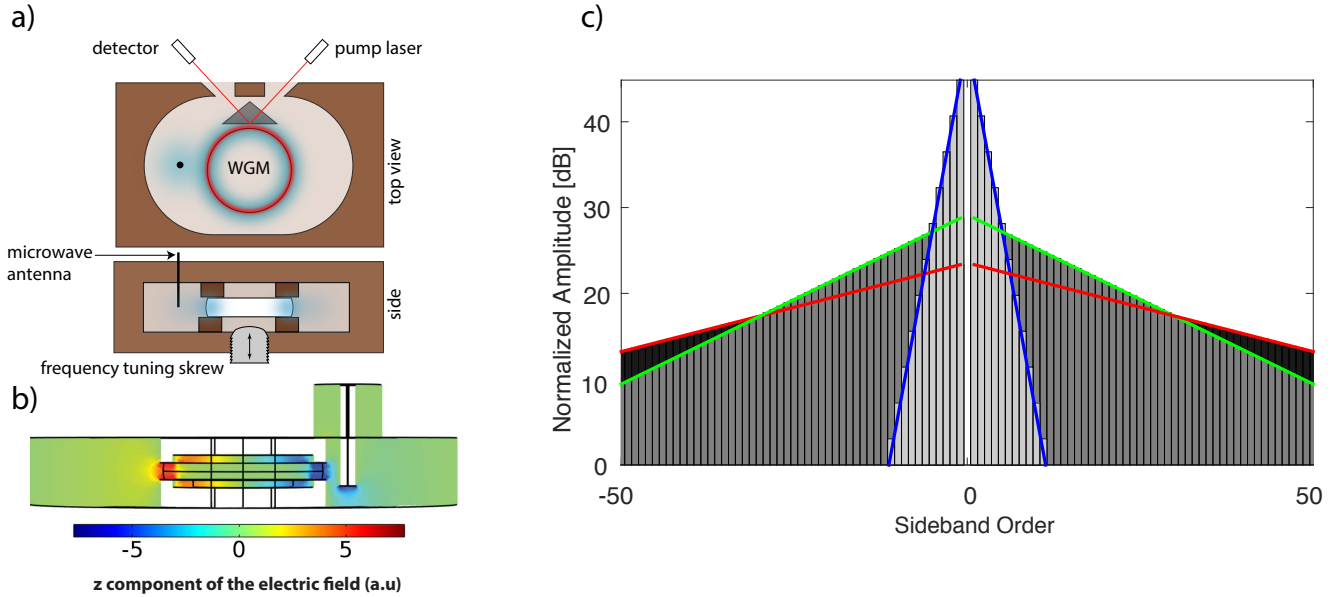


FIG. 2. **Schematic of the proposed frequency comb generator and comb profile** a) Schematic of the WGM clamped between two copper ring electrodes in a 3D microwave cavity. b) Electric field profile of the microwave mode calculated by COMSOL. c) Comb profile for three different parameters $G = 1, 11, 21$ (blue, green, red). Indicating that for larger pump powers the comb gets flatter and wider.

simply either re-designing the 3D microwave cavity or by spreading the comb over multiple FSR.

Due to the very low π -voltage of our system we can highly over-drive the system. For sufficiently high microwave powers this process can cascade into a comb. Due to the presence of two pump fields, the phase and frequency of the generated light are inherently fixed contrary to the usual microresonator Kerr combs. The large number of optical modes separated by equidistant FSR in a mm-sized WGM resonator allows the modulation process to take place not only at the carrier mode, but also at the lower and upper sidebands cascading to generate higher orders sidebands (see Supplement). The formation of higher order sidebands depend on the dimensionless parameter $G = \sqrt{n\Omega}g/\Gamma_o$ which we identify as the ratio of the internal conversion rate over the optical total field loss rate. For weak coupling range ($G \ll 1$) comb formation is suppressed but in the regime ($G > 1$) large combs can be generated. Assuming a system with large number of equidistant optical modes, the output electric field conversion follows [16]:

$$\frac{E_{\text{out}}(t)}{E_{\text{in}}(t)} = \frac{2\frac{\gamma}{\gamma+\gamma'} - 1 - i(\nu + 2G \cos(\Omega t + \phi_\Omega))}{1 + 2iG \cos(\Omega t + \phi_\Omega)}, \quad (3)$$

where γ, γ' stand for the optical coupling and internal field loss rate, respectively, $\nu = \Delta\omega/\Gamma_o$ for the normalized pump detuning, Ω for the microwave frequency and ϕ_Ω for the microwave pump phase. The maximal first order sideband output power is reached in the case of strong over-coupling configuration ($\gamma \gg \gamma'$) with the first order sideband reaching the maximal value of 36% of the

carrier power at $G \approx 0.635$. Moreover, the sidebands' power spectrum of these combs follows an exponential G dependence on the sideband order as follows:

$$P(\omega \pm j\Omega) = \hat{P}_1(G)e^{-B(G)\cdot(j-1)} \text{ for } j \neq 0, \quad (4)$$

where j stands for the sideband order, $\hat{P}_1(G)$ is the first order sideband power and $B(G)$ is the exponential factor and can be approximated to $1/G$. This exponential behaviour of the intensities is expected since j -order sideband works as the carrier for the $j+1$ -order sideband. From this expression follows that the comb gets flatter for high microwave powers (see Fig. 2 c). For a real system the exponential decay is also affected strongly by the nominal refractive index, given by its Sellmeier equation, more than other geometrical factors. This becomes an important factor for long $\chi^{(2)}$ combs in high- Q optical WGM resonators. The output of such system for low values of G follows the same behaviour as a standard phase modulator, where the phase and amplitude of the sidebands are described by the Jacobi expansion in terms of the Bessel functions. Moreover, there is a fixed relation between G and the modulation index (phase-shift amplitude β) of a standard electro-optical modulator $\beta = 4G$ (see Supplement).

Based on the theory proposed here, we built a 3D copper cavity and made a crystalline lithium niobate WGM (see Fig. 3 a). A coherent pump in the telecommunication regime is couple to the fundamental mode of a crystalline WGM resonator. The optical mode is critically coupled using a prism with coupling rates $\gamma = \gamma' = 2\pi \times 346$ kHz. The microwave mode is

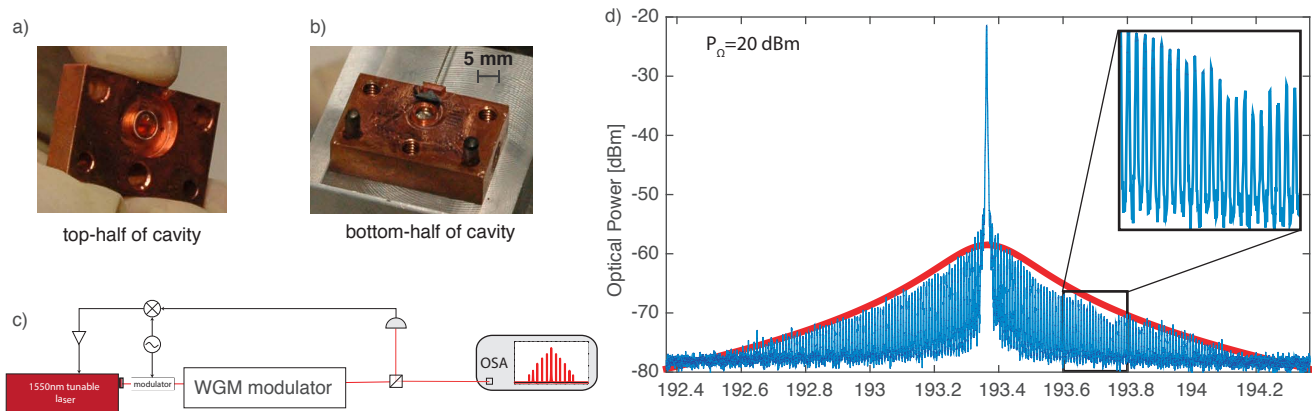


FIG. 3. **Experimental realisation** a) and b) top, and bottom-half of the copper cavity. In the top-half the lithium niobate WGM is mounted. c) Experimental driving scheme of the electro-optic WGM Frequency comb. d) Generation of a frequency comb with 20 dBm microwave power at 8.9 GHz spanning over 100 comb lines. The optical sidebands appear broader as they really are due to the optical spectrum analyzer's (OSA) resolution bandwidth. A theoretical fit of Eq. (4) with detuning due to the dispersion of the lithium niobate. The frequency comb is ≈ 1.6 THz long.

critically coupled at $\Omega_0 = 2\pi \times 8.95$ GHz with a coupling rate $\gamma_\Omega = 2\pi \times 3.6$ MHz and an intrinsic loss rate $\gamma_\Omega = 2\pi \times 16.2$ MHz. Once the optical laser is coupled to the WGM resonator, we send the microwave tone and observe the sidebands on an optical spectrum analyzer (OSA) (see Methods).

If the optical modes are spectrally equidistant, the sidebands are symmetric as predicted in Eq. (3). For microwave powers with ($\gg 1$ mW) corresponding to the regime $G \gg 1$ we can generate multiple sidebands as shown in Fig. 3 d), where we could generate a frequency comb as large as 11 nm for 100 mW (+20 dBm) microwave pump power. The width of the individual comb lines in Fig. 3 d) appear broader than they are due to the OSA best resolution bandwidth of 2.49 GHz. Their actual linewidth corresponds to the width of the optical pump with 0.1 MHz. In comparison to the theoretical description of the envelope in Fig. 2c), the envelope of the comb is not linear in the dB scale as described by Eq. (22). This corresponds to the chromatic dispersion which plays a strong role for long frequency combs since the refractive index does not remain constant, therefore changing the optical FSR. We consider this by adding an increasing detuning with the mode order. We estimate the detuning from each sideband by using the measurable symmetric FSR $\Delta_\pm = |\omega_m - \omega_{m\pm 1}|/2\pi \approx 8.9$ GHz and the mode linewidth ≈ 2 MHz. The detuning for the j -order sideband is given by $|\omega_m - \omega_{m\pm j}|/2\pi - j \cdot \Delta_\pm$. The optical mode has an azimuthal number $m \approx 21660$. Then, it follows for sideband order $j = 30, 60$ and 100 the corresponding detuning of 4.7 MHz, 19 MHz and 54 MHz, respectively. This explains the stronger decay for the higher order sidebands and the extra detuning factor must be added to the envelope presented in Eq. (4).

In summary, we have demonstrated that multi-resonant electro-optic modulation can lead to the forma-

tion of a stable and broadband frequency comb. We theoretically explain the mechanism of the comb formation and describe its spectral features and envelope. As two stabilized sources are used to generate the comb through a second order non-linear effect, the resulting comb lines have a fixed and pre-determined phase relation to each other. We believe that the combination of a compact high quality resonant enhancement with a careful microwave field engineering can become a key concept for power-efficient optical interconnects and extend the range of long distance interconnects due to the inherent phase relation of all the comb lines.

A. Methods

Experiment We fabricate a lithium niobate WGM resonator ($n_o = 2.211$, $n_{eo} = 2.138$, for the ordinary and extra-ordinary polarisation) with $R = 2.45$ mm and minor radius $r = 1.5$ mm, mounted within the copper cavity shown in Fig. 3 a,b). As the optical pump we use a narrow-band tunable laser (DL Pro $\lambda \approx 1550$ nm with a linewidth of 100 kHz) which goes through a polarization controller. Then, the signal is split 99:1, with the weak signal sent to the detector to keep control of the optical power coming from the laser (see Fig. 3 c). The other arm goes to the graded index lens for WGM-prism coupling to a transverse electric mode. We use a silicon prism ($n_{Si} = 3.47$) mounted within the copper cavity. Two holes in the copper cavity allow the optical pump light to enter and the light reflected and the emitted sideband from the WGM resonator to leave the cavity. The power is then collected in the fiber and sent to InGaAs photodetector PDA10CS and its output signal to the oscilloscope. We can use a signal generator to sweep the lasers frequency and scan over the optical modes of the cavity, measure the optical FSR and op-

tical loaded Q using sideband spectroscopy [37]. The microwave signal (R&S-SMR20) is coupled via a coaxial pin coupler introduced close to the WGM resonator inside the cavity. The same transmission line was used for reflection measurements with the vector network analyzer (VNA). A metallic tuning screw is used to perturb the microwave field for fine adjustment of its resonance frequency (see Fig. 2 a). The whole setup is thermally stabilized at room temperature to the mK level with a

proportional-integral-derivative (PID) controller TC200 in combination with temperature sensor (AD590) and a thermoelectric element attached on the outer side of the closed copper cavity. Once the laser is set to the mode, we send the microwave tone and create the sidebands (see Fig. 3 d). These signals are outcoupled through the prism and coupled to the fibers. To measure the sidebands we connect the fiber to the OSA (YOKOGAWA AQ6370C), measuring the reflected pump and the sidebands separately.

-
- [1] J. M. Kahn and D. A. B. Miller, “Communications expands its space,” Jan. 2017.
- [2] J. Pfeifle, V. Brasch, M. Lauerer, Y. Yu, D. Wegner, T. Herr, K. Hartinger, P. Schindler, J. Li, D. Hillerkuss, R. Schmogrow, C. Weimann, R. Holzwarth, W. Freude, J. Leuthold, T. J. Kippenberg, and C. Koos, “Coherent terabit communications with microresonator Kerr frequency combs,” *Nature Photonics*, vol. 8, pp. 375–380, May 2014.
- [3] V. Ataie, E. Temprana, L. Liu, E. Myslivets, B. P.-P. Kuo, N. Alic, and S. Radic, “Ultrahigh Count Coherent WDM Channels Transmission Using Optical Parametric Comb-Based Frequency Synthesizer,” *Journal of Lightwave Technology*, vol. 33, pp. 694–699, Feb. 2015.
- [4] P. Marin-Palomo, J. N. Kemal, M. Karpov, A. Kordts, J. Pfeifle, M. H. P. Pfeiffer, P. Trocha, S. Wolf, V. Brasch, M. H. Anderson, R. Rosenberger, K. Vijayan, W. Freude, T. J. Kippenberg, and C. Koos, “Microresonator-based solitons for massively parallel coherent optical communications,” *Nature*, vol. 546, pp. 274–279, June 2017.
- [5] E. Temprana, E. Myslivets, B. P.-P. Kuo, L. Liu, V. Ataie, N. Alic, and S. Radic, “Overcoming Kerr-induced capacity limit in optical fiber transmission,” *Science*, vol. 348, pp. 1445–1448, June 2015.
- [6] G. Mitchell and H. Hodara, “Review of the 2017 optical fiber communications (ofc) conference,” *Fiber and Integrated Optics*, vol. 36, no. 3, pp. 101–103, 2017.
- [7] M. Imran, P. M. Anandarajah, A. Kaszubowska-Anandarajah, N. Sambo, and L. Poti, “A Survey of Optical Carrier Generation Techniques for Terabit Capacity Elastic Optical Networks,” *IEEE Communications Surveys and Tutorials*, vol. 20, no. 1, pp. 211–263, 2018.
- [8] J. M. Kahn and D. A. Miller, “Communications expands its space,” *Nature Photonics*, vol. 11, no. 1, pp. 5–8, 2017.
- [9] L. W. Luo, N. Ophir, C. P. Chen, L. H. Gabrielli, C. B. Poitras, K. Bergmen, and M. Lipson, “WDM-compatible mode-division multiplexing on a silicon chip,” *Nature Communications*, vol. 5, pp. 1–7, 2014.
- [10] R. Holzwarth, T. Udem, T. W. Hänsch, J. C. Knight, W. J. Wadsworth, and P. S. J. Russell, “Optical frequency synthesizer for precision spectroscopy,” *Physical Review Letters*, vol. 85, no. 11, pp. 2264–2267, 2000.
- [11] W. Liang, D. Eliyahu, V. S. Ilchenko, A. A. Savchenkov, A. B. Matsko, D. Seidel, and L. Maleki, “High spectral purity Kerr frequency comb radio frequency photonic oscillator,” *Nature Communications*, vol. 6, pp. 1–8, 2015.
- [12] J. Pfeifle, V. Brasch, M. Lauerer, Y. Yu, D. Wegner, T. Herr, K. Hartinger, P. Schindler, J. Li, D. Hillerkuss, R. Schmogrow, C. Weimann, R. Holzwarth, W. Freude, J. Leuthold, T. J. Kippenberg, and C. Koos, “Coherent terabit communications with microresonator Kerr frequency combs,” *Nature Photonics*, vol. 8, no. 5, pp. 375–380, 2014.
- [13] M.-G. Suh and K. Vahala, “Gigahertz-repetition-rate soliton microcombs,” *Optica*, vol. 5, pp. 65–66, Jan. 2018.
- [14] T. J. Kippenberg, R. Holzwarth, and S. A. Diddams, “Microresonator-Based Optical Frequency Combs,” *Science*, vol. 332, pp. 555–559, Apr. 2011.
- [15] M. Zhang, C. Wang, B. Buscaino, A. Shams-Ansari, A. Shams-Ansari, J. M. Kahn, and M. Loncar, “Electro-optic Frequency Comb Generation in Ultrahigh-Q Integrated Lithium Niobate Micro-resonators,” in *Conference on Lasers and Electro-Optics (2018), paper FW3E.4*, p. FW3E.4, Optical Society of America, May 2018.
- [16] V. S. Ilchenko, A. A. Savchenkov, A. B. Matsko, and L. Maleki, “Whispering-gallery-mode electro-optic modulator and photonic microwave receiver,” *Journal of the Optical Society of America B*, vol. 20, pp. 333–342, Feb. 2003.
- [17] A. J. Mercante, S. Shi, P. Yao, L. Xie, R. M. Weikle, and D. W. Prather, “Thin film lithium niobate electro-optic modulator with terahertz operating bandwidth,” *Opt. Express*, vol. 26, pp. 14810–14816, May 2018.
- [18] L. Chen, Q. Xu, M. G. Wood, and R. M. Reano, “Hybrid silicon and lithium niobate electro-optical ring modulator,” *Optica*, vol. 1, pp. 112–118, Aug 2014.
- [19] J. Macario, P. Yao, S. Shi, A. Zablocki, C. Harray, R. D. Martin, C. A. Schuetz, and D. W. Prather, “Full spectrum millimeter-wave modulation,” *Opt. Express*, vol. 20, pp. 23623–23629, Oct 2012.
- [20] C. Wang, M. Zhang, B. Stern, M. Lipson, and M. Loncar, “Nanophotonic lithium niobate electro-optic modulators,” *Opt. Express*, vol. 26, pp. 1547–1555, Jan 2018.
- [21] V. Torres-Company and A. M. Weiner, “Optical frequency comb technology for ultra-broadband radio-frequency photonics,” *Laser and Photonics Reviews*, vol. 8, no. 3, pp. 368–393, 2014.
- [22] R. Boyd, *Nonlinear Optics*. Elsevier Science, 2003.
- [23] R. P. Kovacich, U. Sterr, and H. R. Telle, “Short-pulse properties of optical frequency comb generators,” *Applied Optics*, vol. 39, pp. 4372–4376, Aug. 2000.
- [24] Z. Jiang, D. E. Leaird, C. B. Huang, H. Miao, M. Kourogi, K. Imai, and A. M. Weiner, “Spectral Line-by-Line Pulse Shaping on an Optical Frequency Comb Generator,” *IEEE Journal of Quantum Electronics*, vol. 43, pp. 1163–1174, Dec. 2007.
- [25] R. Wu, V. R. Supradeepa, C. M. Long, D. E. Leaird, and A. M. Weiner, “Generation of very flat optical frequency

- combs from continuous-wave lasers using cascaded intensity and phase modulators driven by tailored radio frequency waveforms,” *Optics Letters*, vol. 35, pp. 3234–3236, Oct. 2010.
- [26] K. Beha, D. C. Cole, P. Del’Haye, A. Coillet, S. A. Diddams, and S. B. Papp, “Electronic synthesis of light,” *Optica*, vol. 4, pp. 406–411, Apr. 2017.
- [27] D. V. Strekalov, C. Marquardt, A. B. Matsko, H. G. L. Schwefel, and G. Leuchs, “Nonlinear and quantum optics with whispering gallery resonators,” *Journal of Optics*, vol. 18, no. 12, p. 123002, 2016.
- [28] A. Rueda, F. Sedlmeir, M. C. Collodo, U. Vogl, B. Stiller, G. Schunk, D. V. Strekalov, C. Marquardt, J. M. Fink, O. Painter, G. Leuchs, and H. G. L. Schwefel, “Efficient microwave to optical photon conversion: an electro-optical realization,” *Optica*, vol. 3, pp. 597–604, Jun 2016.
- [29] D. V. Strekalov, H. G. L. Schwefel, A. A. Savchenkov, A. B. Matsko, L. J. Wang, and N. Yu, “Microwave whispering-gallery resonator for efficient optical up-conversion,” *Physical Review A*, vol. 80, no. 3, pp. 033810–5, 2009.
- [30] M. Leidinger, S. Fieberg, N. Waasem, F. Kühnemann, K. Buse, and I. Breunig, “Comparative study on three highly sensitive absorption measurement techniques characterizing lithium niobate over its entire transparent spectral range,” *Opt. Express*, vol. 23, pp. 21690–21705, Aug 2015.
- [31] G. Schunk, J. U. Fürst, M. Förtsch, D. V. Strekalov, U. Vogl, F. Sedlmeir, H. G. L. Schwefel, G. Leuchs, and C. Marquardt, “Identifying modes of large whispering-gallery mode resonators from the spectrum and emission pattern,” *Opt. Express*, vol. 22, pp. 30795–30806, Dec 2014.
- [32] I. Breunig, B. Sturman, F. Sedlmeir, H. G. L. Schwefel, and K. Buse, “Whispering gallery modes at the rim of an axisymmetric optical resonator: Analytical versus numerical description and comparison with experiment,” *Opt. Express*, vol. 21, pp. 30683–30692, Dec 2013.
- [33] I. S. Grudin, A. B. Matsko, A. A. Savchenkov, D. Strekalov, V. S. Ilchenko, and L. Maleki, “Ultra high Q crystalline microcavities,” *Optics Communications*, vol. 265, pp. 33–38, Sept. 2006.
- [34] M. Goryachev, N. Kostylev, and M. E. Tobar, “Single-photon level study of microwave properties of lithium niobate at millikelvin temperatures,” *Physical Review B*, vol. 92, p. 060406, Aug. 2015.
- [35] J. U. Fürst, D. V. Strekalov, D. Elser, M. Lassen, U. L. Andersen, C. Marquardt, and G. Leuchs, “Naturally phase-matched second-harmonic generation in a whispering-gallery-mode resonator,” *Phys. Rev. Lett.*, vol. 104, p. 153901, Apr 2010.
- [36] M. Tsang, “Cavity quantum electro-optics,” *Physical Review A*, vol. 81, p. 063837, June 2010.
- [37] J. Li, H. Lee, K. Y. Yang, and K. J. Vahala, “Sideband spectroscopy and dispersion measurement in microcavities,” *Opt. Express*, vol. 20, pp. 26337–26344, Nov 2012.
- [38] M. R. Foreman, F. Sedlmeir, H. G. L. Schwefel, and G. Leuchs, “Dielectric tuning and coupling of whispering gallery modes using an anisotropic prism,” *J. Opt. Soc. Am. B*, vol. 33, pp. 2177–2195, Nov 2016.
- [39] Y. A. Demchenko and M. L. Gorodetsky, “Analytical estimates of eigenfrequencies, dispersion, and field distribution in whispering gallery resonators,” *J. Opt. Soc. Am. B*, vol. 30, pp. 3056–3063, Nov 2013.
- [40] Y. R. Shen, “Permutation symmetry of nonlinear susceptibilities and energy relation,” *Phys. Rev.*, vol. 167, pp. 818–821, Mar 1968.
- [41] C. K. Law, “Effective hamiltonian for the radiation in a cavity with a moving mirror and a time-varying dielectric medium,” *Phys. Rev. A*, vol. 49, pp. 433–437, Jan 1994.
- [42] P. Hobbs, *Building Electro-Optical Systems: Making It all Work*. Wiley Series in Pure and Applied Optics, Wiley, 2011.

I. SUPPLEMENTARY MATERIAL

A. Optical Whispering Gallery Modes & Dispersion

A whispering gallery mode resonator consist of a usually round dielectric material with refractive index n higher than its surrounding [27]. At an angle beyond the critical angle the light undergoes total internal reflection and all the light is reflected. Light can be coupled into the WGM through an evanescent field coupler such as a prism. In a physical resonator loss is always present and we distinguish between intrinsic loss γ' and coupling loss γ due to the interaction of the prism. If the resonator is critically coupled the coupling loss equals the intrinsic loss $\gamma' = \gamma$ and all the light is coupled into the resonator. The total loss is $\Gamma = \gamma + \gamma'$. In a prism coupled WGM system we have control over the coupling loss γ by adjusting the distance of the prism from the resonator. Through careful adjustment, we can over-couple $\gamma' < \gamma$ and under-couple $\gamma' > \gamma$ the resonator. The loss is related to the lifetime of the light in the resonator $\tau_p = 1/2\Gamma$ considering that the coupling rates are defined for the field. The quality factor is $Q = \omega\tau_p$, where ω is the frequency of the light at the resonant position. The free spectral range corresponds to the inverse of the roundtrip time $\text{FSR} = 1/\tau = 2\pi nR/c$, R and c are the radius and the speed of light, respectively.

In a linear resonator the resonant frequency simply follows from the argument that an integer number of wavelengths needs to fit into the optical path length $\lambda_0 = 2\pi nR/m$ or equivalently $\omega = 2\pi \cdot m \cdot \text{FSR}$ and $nk_0 = m/R$, with the wavenumber in free space $k_0 = \omega/c$. For very large WGM resonators this might still be a valid expression. It does not however take the actual geometric dispersion seen from a three dimensional WGM into account. In order to find better expressions for WGM resonators we need to consider the Helmholtz equation, with the appropriate geometry. Here we choose a local toroidal coordinates system following Ref. [32, 38]. In such coordinates the scalar field inside of the resonator and outside of the resonator can be written as:

$$\mathbf{E}_{q,p,m}^\nu(\mathbf{r}) \approx \begin{cases} E_0 \exp(-\frac{\theta^2}{2\theta_m^2}) H_p(\frac{\theta}{\theta_m}) \text{Ai}[f_{m,q}^\nu(\rho)] e^{im\varphi} & \text{if } \rho < P \\ A_\nu \exp(-\frac{\theta^2}{2\theta_m^2}) H_p(\frac{\theta}{\theta_m}) \exp(-\kappa(\rho - P)) e^{im\varphi} & \text{if } \rho > P, \end{cases} \quad (5)$$

where r is the position relative to the cylindrical coordinates origin. ρ and θ stand for the distance and polar angle relative to the center of the curvature of the rim. ν is the polarisation index parallel (TE) and orthogonal (TM) to the symmetry axis, $\kappa_\nu = k_0 \sqrt{n_\nu^2 - 1}$ the evanescent decay constant. $q = \{1, 2, \dots\}$ is the radial number which is the number of maxima of the electric field intensity along the \hat{r} axis. $p = \{0, 1, \dots\}$ stands the polar number and $m = \{1, 2, \dots\}$ is the azimuthal number representing the number of the electric field amplitude maxima along $\hat{\varphi}$. H_p are the Hermite polynomials of degree p which determine the lateral mode profile. The Airy function determines the radial distribution of the electric field in the resonator. E_0 is a normalization constant and A_ν is the evanescence field amplitude given by the boundary conditions according to each polarization. The abbreviations in the formula are defined as

$$f_m^\nu(\rho) = (P + \Delta_\nu - \rho)/u_m - \alpha_q, \quad (6a)$$

$$\theta_m = (\tilde{R}_\nu/P)^{3/4} \frac{1}{\sqrt{m}}, \quad (6b)$$

$$u_m = 2^{-1/3} m^{-2/3} \tilde{R}_\nu, \quad (6c)$$

where α_q is the q -root of the Airy function (i.e. $\text{Ai}(-\alpha_q) = 0$) and $\tilde{R} = R + \Delta_\nu$ is the effective radius. The functions u_m is related to the width and position of the mode maxima along the \hat{r} -axis inside the resonator.

The previous considerations give an account for the spatial description of the field but do not reveal the spectral resonance positions. For this we use the dispersion relation [38, 39]:

$$\omega_{q,p,m}^\nu \frac{n_\nu \tilde{R}_\nu}{c} = l - \alpha_q \left(\frac{l}{2} \right)^{1/3} + \frac{2p(\sqrt{\tilde{R}_\nu} - \sqrt{P}) + \sqrt{\tilde{R}_\nu}}{2\sqrt{P}} - \frac{\zeta n}{\sqrt{n^2 - 1}} + \frac{3\alpha_q^2}{20} \left(\frac{l}{2} \right)^{-1/3} - \frac{\alpha_q}{12} \left(\frac{2p(\tilde{R}_\nu^{3/2} - P^{3/2}) + \tilde{R}_\nu^{3/2}}{P^{3/2}} \cdot \frac{2n\zeta(2\zeta^2 - 3n^2)}{(n^2 - 1)^{3/2}} \right) \left(\frac{l}{2} \right)^{-2/3} + \mathcal{O}(l^{-1}) \quad (7)$$

with $l = p + m$ and $\zeta = 1$ for TE and n^{-2} for TM modes. The first part clearly relates to the standard Fabry-Perot Equation and the higher order contributions take the effects of the geometry into account. The optical FSR between modes of the same family $\{p,q\}$ will remain constant for several GHz but a small dispersion contribution coming mainly from the term $\propto (l^{1/3})$ and the change in the nominal refractive index $n(\omega)$ (following a Sellmeier equation).

B. Second order interaction

The time averaged stored energy U of j electromagnetic waves due to the second order electric susceptibility $\chi^{(2)}$ which relates the polarization $P_j^{(2)} = \chi_{jil}^{(2)} E_i E_l$ to the electric field E can be summarised in the following expression [40]:

$$\langle U^{(2)} \rangle = \sum_j \int dV \int dt \left\langle \mathbf{E}_j \cdot \frac{\partial \mathbf{P}_j^{(2)}}{\partial t} \right\rangle. \quad (8)$$

The interaction Hamiltonian can be derived from this expression using the electric field operator in the second quantization which are given as: $\hat{\mathbf{E}}_j(\mathbf{r}, t) = i\sqrt{\frac{\hbar\omega}{2\epsilon_j V_j}} (\psi_j(\mathbf{r}) \hat{a}_j e^{-i\omega_j t} - \psi_j^\dagger(\mathbf{r}) \hat{a}_j^\dagger e^{i\omega_j t}) \mathbf{e}$, where ψ_j is the spatial mode distribution, \mathbf{e} the polarization direction, V_j is the effective mode volume, ϵ_j the permittivity, and a_j (a_j^\dagger) stand for the annihilation (creation) operator, respectively. The Hamilton operator for this interaction is found by rewriting Eq. (8) using the electric field operators and assuming the energy conservation condition of $\omega_3 = \omega_1 + \omega_2$. Then, it follows

$$\hat{H}_{\text{int}} = 2\epsilon_0 \chi_{\text{eff}}^{(2)} \sqrt{\frac{\hbar^3 \omega_1 \omega_2 \omega_3}{8\epsilon_1 \epsilon_2 \epsilon_3 V_1 V_2 V_3}} \int dV (\psi_3^\dagger \psi_2 \psi_1 \hat{a}_3^\dagger \hat{a}_2 \hat{a}_1 + \psi_3 \psi_2^\dagger \psi_1^\dagger \hat{a}_3 \hat{a}_2^\dagger \hat{a}_1^\dagger). \quad (9)$$

The first term inside the integral contains the operators for the creation of a photon ω_3 from the annihilation of two photons with frequencies ω_1 and ω_2 . On the other hand, the second term contains the decay of ω_3 into ω_1 and ω_2 . Both processes in the Hamiltonian set the bidirectionality of this effect and their symmetry relies on the symmetry of $\chi^{(2)}$. The quantized energy for this interaction is given by the single photon electric field amplitudes and their mode overlap. Defining the three single photon interaction energy as $\hbar g$ follows

$$\hat{H}_{\text{int}} = \hbar g (\hat{a}_3^\dagger \hat{a}_2 \hat{a}_1 + H.c.) = 2\epsilon_0 \chi_{\text{eff}}^{(2)} \sqrt{\frac{\hbar^3 \omega_1 \omega_2 \omega_3}{8\epsilon_1 \epsilon_2 \epsilon_3 V_1 V_2 V_3}} \int dV (\psi_3^\dagger \psi_2 \psi_1 \hat{a}_3^\dagger \hat{a}_2 \hat{a}_1 + H.c.), \quad (10)$$

where g is commonly known as the second order non-linear coupling constant given by:

$$g = 2\epsilon_0 \chi^{(2)} \sqrt{\frac{\hbar \omega_1 \omega_2 \omega_3}{8\epsilon_1 \epsilon_2 \epsilon_3 V_1 V_2 V_3}} \int dV \psi_3^\dagger \psi_2 \psi_1. \quad (11)$$

For a fixed value of $\chi^{(2)}$, which is purely material dependent, the amplitude of g is determined by the geometry and its maximal value in full mode overlap is set by $\propto V^{-1/2}$. In a closed system with real $\chi^{(2)}$, g is also real which means that the energy between the participating fields only oscillates with the frequency g . For the special case that one of the modes is a bright coherent field (classical field: $\hat{a}_1 \rightarrow \alpha = \sqrt{n_p} e^{i\phi}$) and no kind of depletion of this field over the relevant time scale, the Hamiltonian becomes:

$$\hat{H}_{\text{int}} = \hbar \alpha g (\hat{a}_3^\dagger \hat{a}_2 e^{i\phi} + \hat{a}_3 \hat{a}_2^\dagger e^{-i\phi}). \quad (12)$$

This is known as the beam splitter Hamiltonian and αg is understood as the photon conversion rate from the field a_2 to the field a_3 and vice versa. The result of this kind of linearisation of the Hamiltonian is known as the zero-photon process characterized by photons scattering from one mode into another without changing the total number of photons [41]. In the case of a group of modes ω_u , equidistantly separated by the strong coherent field frequency, the Hamiltonian can be written as:

$$\hat{H}_{\text{int}} = \hbar \alpha g \sum_{u=-N}^{N-1} (\hat{a}_u \hat{a}_{u+1}^\dagger e^{i\phi} + \hat{a}_u^\dagger \hat{a}_{u+1} e^{-i\phi}). \quad (13)$$

where $2N + 1$ is the number of modes involved in the system.

To estimate the non-linear coupling constant in our system we rely on the COMSOL numerical simulations, optimizing the microwave cavity geometry such as WGM resonator size, ring thickness, etc. From these simulations we extract information such as the microwave resonance frequency, microwave internal Q'_Ω factor, microwave coupling rate, microwave mode volume and the microwave single photon electric field for different disk thickness h and the mode profile $m = 1$. In the simulation we try to keep the reference microwave resonance frequency at 9.3 GHz and

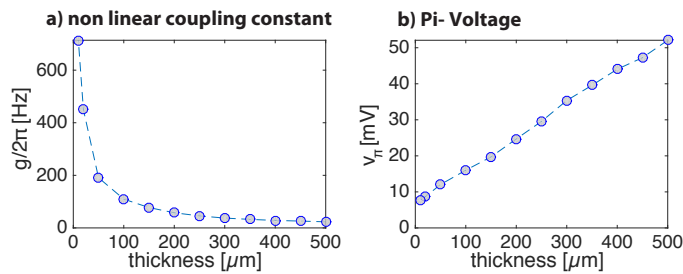


FIG. 4. Values from the simulation of the 3D WGM resonator system. a) Non-linear coupling constant g as a function of the WGM resonator thickness. b) V_π as a function of the WGM resonator thickness.

we have gradually changed the geometry according to the resonator thickness to match this desired frequency. The simulated values of the non-linear coupling constant are shown in Fig. 4 a). This value as well as the single photon electric field E_Ω scales with $V^{-1/2}$ according to Eq. (11). In our system it scales as $\sim h^{-1}$ due to the change of the ring thickness to keep the resonance frequency constant. It is worth to point out that the values shown from the simulation are referential since there are many configurations for changing cavity dimensions to keep the frequency constant. In the simulated range the values for g go from $2\pi \times 23$ Hz to $2\pi \times 713$ Hz. These values can be improved by reducing the ring thickness even more and increasing the cavity volume to keep the frequency fixed. This would also increase of the system's sensitivity to air gaps and small changes on the ring electrodes' geometry.

In our simulations the intrinsic γ'_Ω value depends on the material (lithium niobate) dielectric loss, geometry and finite conductivity of metal (copper). The current density is highly confined on the ring electrodes surfaces, where the current is at its maximum amplitude in the front and back part of the ring electrodes where the electric fields is at its minima for the mode $m = 1$. Because of this, the roughness of the ring surface becomes the most relevant part in the fabrication of this kind of cavities.

C. Efficiency and π -Voltage

The efficiency of an electro-optic device can be given in terms of V_π . This is the voltage applied to an electro-optic phase modulator to create a π phase shift to the optical carrier. We can extract this information from the non-linear coupling constant g which can be defined as the phase shift induced to the optical carrier by a single microwave photon per roundtrip [36]:

$$\frac{\Delta\phi}{\tau} = g. \quad (14)$$

Moreover, the classical field amplitude α in case of a resonant system is given in terms of the input power P_{AC} as:

$$n_\alpha = |\alpha|^2 = \frac{2\gamma P_{AC}}{\hbar\omega((\gamma + \gamma')^2 + \Delta\omega^2)}, \quad (15)$$

where n_α is the mean photon number in the mode. The standard relation between power and a sinusoidal peak voltage V_p in a standard AC circuit holds:

$$P_{AC} = \text{Re} \left(\frac{V_p^2}{2Z} \right), \quad (16)$$

where Z is the load impedance which in most of the cases is 50 Ohm. In the optical resonator the carrier stays an average time τ_p before it is outcoupled or absorbed. We find the voltage V_π by rewriting the relation $\alpha g \tau_p = \pi$ in terms of the voltage and it follows:

$$V_\pi = \frac{\pi}{g\tau_p} \sqrt{\frac{Z\hbar\Omega(\gamma + \gamma')^2}{\gamma}}. \quad (17)$$

D. $\chi^{(2)}$ -comb generation

To describe the dynamics of a system with $2N + 1$ optical modes equally separated under the presence of a resonant microwave drive, the equations of motion are

$$\dot{a}_u = \frac{i}{\hbar} [\hat{H}_{\text{int}}, a_u] = -i\sqrt{n_\Omega}g(a_{u-1}e^{i\phi_\Omega} + a_{u+1}e^{-i\phi_\Omega}). \quad (18)$$

For a microwave resonant system with the field rate for the coupling and internal loss rates given by γ_Ω and γ'_Ω , the photon number can be calculated as $n_\Omega = 2\gamma_\Omega P_\Omega / \hbar\Omega(\gamma_\Omega + \gamma'_\Omega)^2$, where P_Ω stands for the input power. Under the presence of an optical drive at mode u' and assuming that all the optical modes share the same coupling γ and internal loss rates γ' Eq. (18) in the rotation frame becomes:

$$\dot{\tilde{a}}_u = -(\Delta\omega_u + \gamma + \gamma')\tilde{a}_u - i\sqrt{n_\Omega}g(\tilde{a}_{u-1}e^{i\phi_\Omega} + \tilde{a}_{u+1}e^{-i\phi_\Omega}) + \sqrt{2\gamma}A\delta(\omega_u - \omega_{u'}), \quad (19)$$

where $\Delta\omega_u = (\omega + (u - u')\Omega) - (\omega_{u'} + (u - u') \cdot \text{FSR})$ is the detuning between the signal and the mode u and $A = \sqrt{P/\hbar\omega}$ represents a monochromatic driving field. The equation describes the intuitive picture that the optical power of a given sideband is the pump for the next order sideband and so on. Then it follows that the contribution of each mode to the system's energy decreases exponentially with its order. We profit from this feature to give a solution to these equations. Then, for a finite number of modes ($N \gg 1$), we can approximate the system to have an infinite number of modes ($N \rightarrow \infty$), allowing an analytical solution to Eq. (19) in the steady state. Moreover, we assume g is a real quantity because we are working with pure phase modulation ($\text{Im}(\chi^{(2)}) = 0$). For the case of the microwave tone frequency matching the optical FSR, the solution to Eq. (19) is given by:

$$E_{\text{out}}(t) = \frac{2\gamma/\Gamma - 1 - i(\nu + 2G \cos(\Omega t + \phi_\Omega))}{1 + 2iG \cos(\Omega t + \phi_\Omega)} E_{\text{in}}(t). \quad (20)$$

This extended expression from Ref. [16] contains the whole information of the system such as intensity and phase of the sidebands. For an initially strongly overcoupled configuration, that maximizes the amplitude of sidebands, and full resonance condition. The last equation becomes:

$$E_{\text{out}}(t) = \exp[-2i \arctan(2S \cos(\Omega t + \phi_\Omega))] E_{\text{in}}(t). \quad (21)$$

It is worth to compare this expression with the electric field output of a non resonant phase modulator which is given by:

$$\begin{aligned} E_{\text{out}}(t) &= \exp[-i\beta \cos(\Omega t)] E_{\text{in}}(t) \\ &= E_{\text{in}}(t) \sum_{l=-\infty}^{\infty} (-i)^l j_l(\beta) e^{-il\Omega t}, \end{aligned} \quad (22)$$

where j_l are the usual l -th order Bessel functions of first kind and β is the modulation index. Both expressions coincide for small values of G where the small angle approximation $\arctan(x) \approx x$ holds. From this comparison, we find the equivalence of the G parameter to the modulation index given by $\beta = 4G$ and the relation between the phases of the sidebands relative to the carrier [42], which holds for any modulation power.

In Fig. 1 c) we show a frequency comb with $G = 5$, where the sidebands' powers follow an exponential envelope as described in Eq. (4). In our system the maximum power of the first order sideband $P^{(1)*}/P_{\text{in}} = 0.36$ for $G \approx 0.64$. This value depends on the number of the optical modes involved. For example, for three optical modes the first sideband maximal normalized power is 0.5 at $G = 0.5$.